# Evaluation of Permanent Magnet Distribution Schemes for Toroid Power Inductor with Increased Saturation Current Using 3D Physical Models

Zhiyong Xia, *Student Member*, *IEEE*, Jaber A. Abu Qahouq, *Senior Member, IEEE*, and Sushma Kotru, *Senior Member, IEEE*

The University of Alabama
Department of Electrical and Computer Engineering
Tuscaloosa, Alabama 35487, USA

***Abstract*—Effects of different permanent magnet (PM) distribution schemes on the saturation performance of a permanent magnet toroid power inductor are presented and evaluated in this paper. By appropriately placing the PM in the gap of the power inductor, the flux induced by the winding current can be cancelled partially or completely by the flux induced by one or multiple PM pieces. This can lead to increase in the saturation current of the power inductor. Multi-PM distribution schemes are proposed for a power inductor in order to allow for improved and more uniform flux cancellation and therefore higher saturation current. Several PM distribution patterns in the power inductor are evaluated using results obtained from 3D physical models which are developed using ANSYS/Maxwell. The distribution schemes are compared in terms of their effects on the performance metrics of the power inductor. By appropriately selecting or tuning the air gap sizes and the PM dimensions using the 3D physical models in this paper, the multi-PM distribution method can yield higher saturation current with almost no drop in the inductance value.**

***Keywords—Power inductor, permanent magnet (PM), saturation current, ferrite, NdFeB magnet, finite-element analysis, dc-dc, converter, power electronics, magnetics.***

## I. Introduction

The power inductor is the biggest discrete component and indispensable part of most switching power converters, which are used in many applications, and its performance affects the performance of these converters and applications in many aspects, such as switching ripple, power losses, bandwidth, stability and dynamic performance [1-24]. The inductance value and saturation current are two key performance indicators of power inductor. High inductance density and high saturation current are desirable which are important requirements in a high power density application. Several efforts have been made to increase the inductance density and the saturation current of power inductors. One of these methods as presented in [3], among other references, is to insert a permanent magnet (PM) into the airgap of the core of the power inductor. The flux induced by this PM can cancel the flux induced by the winding current, which can increase the saturation current of power inductor without significantly affecting the inductance value. However, the effect of the distribution schemes or patterns of PM on the performance of power inductor has not been investigated in [3] and other similar works.

In this work, instead of using a single PM, multiple PMs distribution scheme for power inductor design is utilized. Multiple PMs are inserted in multiple distributed airgaps in the soft magnet core. This distribution of the PMs affects the magnetic field produced by PM, and therefore it can affect the flux cancellation and saturation current. The work presented in this paper focuses on improving the effectiveness and uniformity in flux cancellation in order to increases the saturation current when using multiple PMs for the design of power inductor. Several power inductor designs with various PM distribution schemes are evaluated through ANSYS/Maxwell 3D physical modeling and simulation to illustrate the design principal.

The multi-PM distribution concept for power inductors and the design examples for illustration and comparison are illustrated in section II. Section III presents the 3D physical simulation results of several different toroid inductors with different PM distribution patterns and compares or evaluates the performances among these toroid inductor designs. The conclusions are presented in Section IV.

## II. Toroid Power Inductors with Distributed Permanent Magnets Schemes

The proposed distributed PM scheme refers to the design structure, which evenly inserts several PMs into the airgaps of power inductor. This structure affects the distribution of magnetic field induced by the PMs. By properly placing the PMs in the airgaps and tuning the size of the airgaps, a uniform magnetic field without significantly affecting its intensity can be obtained. This uniform magnetic field allows for better flux cancellation which can increase the saturation current of power inductor with slight effect on the inductance value.

Fig. 1a shows an illustration diagram for a toroid core (soft magnet, e.g. ferrite) with a single gap that includes a relatively small PM piece, as presented in [3]. Fig. 1b shows a diagram

illustrating the proposed toroid core with two gaps each of which includes a relatively small PM piece (two PM pieces total). This PM distribution concept can be realized with more than two gaps and/or more than two PM pieces. The main objective in this paper is to evaluate whether different PM distribution scenarios can affect the performance metrics of the power inductors especially saturation current and inductance value.

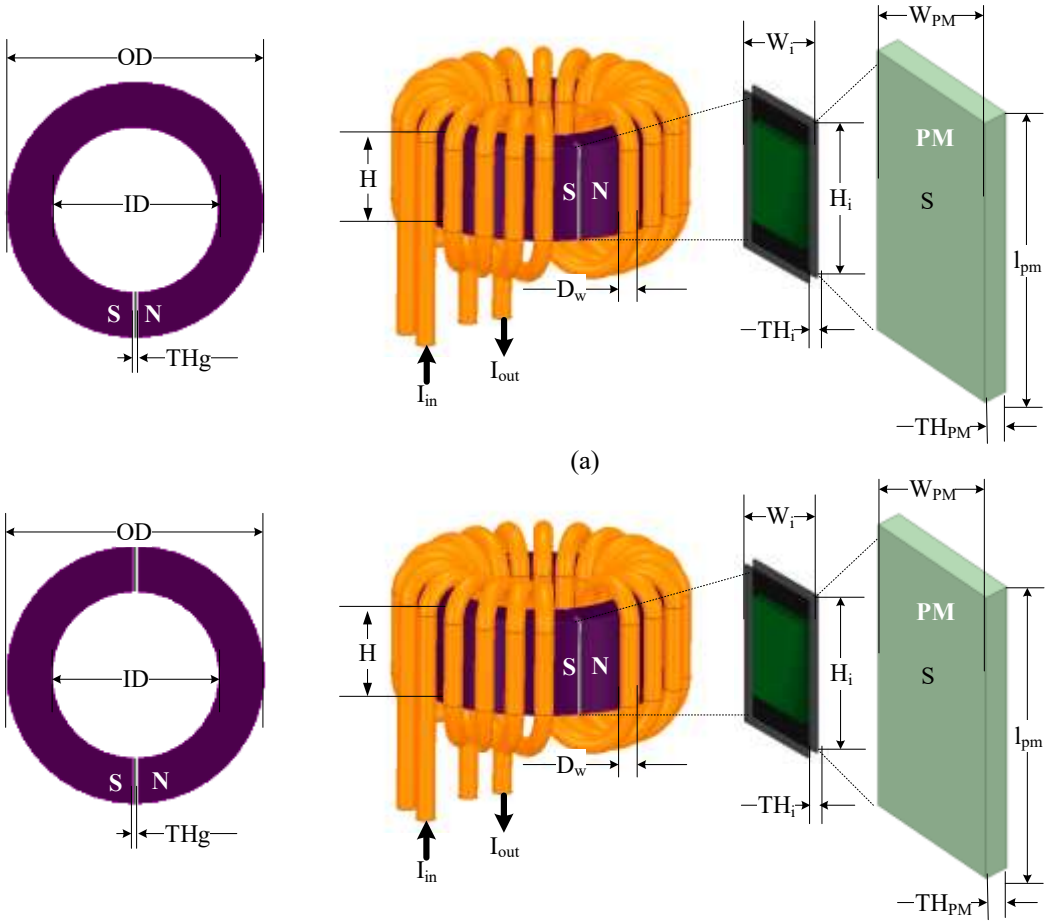


Fig. 1. The design specifications and 3-D physical models of TPIs: (a) PM-TPI and (b) DPM-TPI-1 and DPM-TPI-2.

In this work, three toroid power inductors (TPIs) with three different PM distributions are designed, i.e. PM-TPI, DPM-TPI-1 and DPM-TPI-2 (see Fig. 1 and Table I). The simulation or evaluation results for the models (of the three designs) developed using ANSYS/Maxwell software are presented in the next section. PM-TPI has one PM piece inserted in one gap and DPM-TPI-1 has two small pieces of PM distributed in two gaps while maintaining the total volume of these two gaps be equal to the single gap volume of PM-TPI. DPM-TPI-2 also has two small pieces of PM inserted in the two gaps, but the total volume of these two gaps is 81% of the gap volume in PM-TPI or the gaps volume in DPM-TPI-1. However, the total volume of PM pieces is kept equal for PM-TPI, DPM-TPI-1 and DPM-TPI-2. The design specifications for each of the three power inductors are shown in Fig. 1 and Table I.

The ferrite material of the toroid core is 3C96 with $\mu_r \approx$ 5500, $B_{sat} \approx 0.4$ T at 25℃ in the first quadrant, and the conductivity is 0.2 s/m) [25]. The PM material utilized is NdFeB-N35EH, whose residual flux density $B_r$ is 1.06 T, coercivity $H_c$ is 574.8 KA/m, intrinsic coercivity $H_{ci}$ is 2244.8 KA/m, and the maximum energy product $(BH)_{max}$ is 188 KJ/m$^3$ [26]. Two copper wires with the size of AWG16 are paralleled to form the winding of the power inductor.

## III. ANSYS/MAXWELL 3-D Simulation Results for Multi-TPIs

The three different TPIs designs are modelled in ANSYS/MAXWELL software package based on the design specifications given in the section II. The related 3-D physical model simulation results of these TPIs under different operation points are shown in Fig. 2 and Table II. Fig. 2 shows the flux density (B) magnitude for each core in the three power inductors when the DC current is swept from 0A to 14A for

PM-TPI and from 0A to 18A for DPM-TPI-1 and DPM-TPI-2. For all three different designs, the net flux has the same trend, i.e. the net flux first decreases as the DC current increases starting from 0A, and then increases when the DC current continues to increase beyond a given value at which the net flux becomes approximately zero. This is attributed to the presence of one or more PMs in one or more gaps of the core of each power inductor. The flux induced by the winding's current is cancelled by the flux induced by one or multiple PM pieces.

TABLE I
The design specifications of the three TPIs (Fig. 1)

| Parameters | PM-TPI | DPM-TPI-1 | DPM-TPI-2 | Units | Description |
|---|---|---|---|---|---|
| OD | 17 | 17 | 17 | mm | Outer diameter of core |
| ID | 11 | 11 | 11 | mm | Inner diameter of core |
| H | 6.4 | 6.4 | 6.4 | mm | Height of core |
| $TH_g$ | 0.6 | 0.3 | 0.24 | mm | Length of gap |
| $TH_{pm}$ | 0.3 | 0.15 | 0.15 | mm | Thickness of PM |
| $W_{pm}$ | 2.4 | 2.4 | 2.4 | mm | Width of PM |
| $l_{pm}$ | 4 | 4 | 4 | mm | Length of PM |
| $H_i$ | 6.4 | 6.4 | 6.4 | mm | Height of insulator |
| $W_i$ | 3 | 3 | 3 | mm | Width of insulator |
| $TH_i$ | 0.3 | 0.15 | 0.09 | mm | Thickness of insulator |
| N | 10 | 10 | 10 | -- | Number of winding turns |
| $D_w$ | 1.29 | 1.29 | 1.29 | mm | Diameter of copper wire |
| $T_{core}$ | 3C96 | | | -- | Material type of core |
| $T_{pm}$ | NdFeB-N35EH | | | -- | Material of PM |

For PM-TPI, the winding flux at 7 A is cancelled almost completely by the flux from the single PM flux, and the core becomes partially saturated at 14A. The inductance value of the PM-TPI is ~8.38 μH. For the DPM-TPI-1, the net flux is almost 0 at 9A, and the core is partially saturated at 18A. It can be observed that the saturation current for DPM-TPI-1 (with distributed PMs) increases from 14A to 18A (by ~29%) compared with PM-TPI (with a single PM), but its inductance value drops from ~8.38 μH to ~6.94 μH. The only difference between PM-TPI and DPM-TPI-1 is that the PMs in the DPM-TPI-1 are separated into two parts and evenly distributed inside the two gaps in the power inductor. This difference leads to the increase in the saturation current from 14 A to 18 A as a result of better uniform flux cancellation in the core of DPM-TPI-1. However, the inductance value deceases by ~17%. Thus in the DPM-TPI-1 design case there is a trade-off between the saturation current value and the inductance value which the next discussion shows how to reduce.

In order to reduce the effect on the inductance value while increasing the saturation current simultaneously, the volume of the gaps in the core of the DPM-TPI-2 design is reduced to 81% of that for the PM-TPI design or the DPM-TPI-1 design. Based on Fig. 2(c) and Table II, it can be observed that the inductance value for the DPM-TPI-2 is 8.3 μH, which is close to the inductance value of PM-TPI (8.38 μH), while still being able to increase the saturation current from 14 A to 18 A. It can also be observed that the flux distribution in the core of DPM-TPI-2 is more uniform.

An analysis of these results suggest that when using the PM distribution concept higher saturation current can be achieved with almost no decrease in the inductance value. The distribution can be controlled such that additional increase in saturation current is achieved at the cost of some reduction in the inductance value.

TABLE II
Comparison between the three TPI designs with different PM distributions

| | PM-TPI | DPM-TPI-1 | DPM-TPI-2 |
|---|---|---|---|
| Volume of power inductor | 1452 | 1452 | 1452 |
| Footprint size of inductor | 3.83 | 3.83 | 3.83 |
| Inductance (μH) | 8.38 | 6.94 | 8.30 |
| Inductance density | 2.19 | 1.81 | 2.17 |
| Saturation current Isat (A) | 14 | 18 | 17-18 |
| Current density @ Isat | 3.66 | 4.70 | 4.70 |

Fig. 3 shows the changes in the vector of flux density (i.e. B) for the DPM-TPI-2 design when the DC current increases from 0A to 18A. It can be observed that when the current increases from 0 A to 9A, the vector of B flows in counterclockwise direction, and when the current increases beyond 9 A, the direction of the vector of B is changed to the clockwise direction. This is because from 0A and 9A, the magnetic field by the PM is dominant (larger than the field from the current carrying winding), and above 9 A, the magnetic field induced by the current carrying winding is dominant. The magnitude changes of flux density in Fig. 3 is consistent with the case in Fig. 2. The vectors of flux density for the PM-TPI and the DPM-TPI-1 have the same trend as for the DPM-TPI-2.

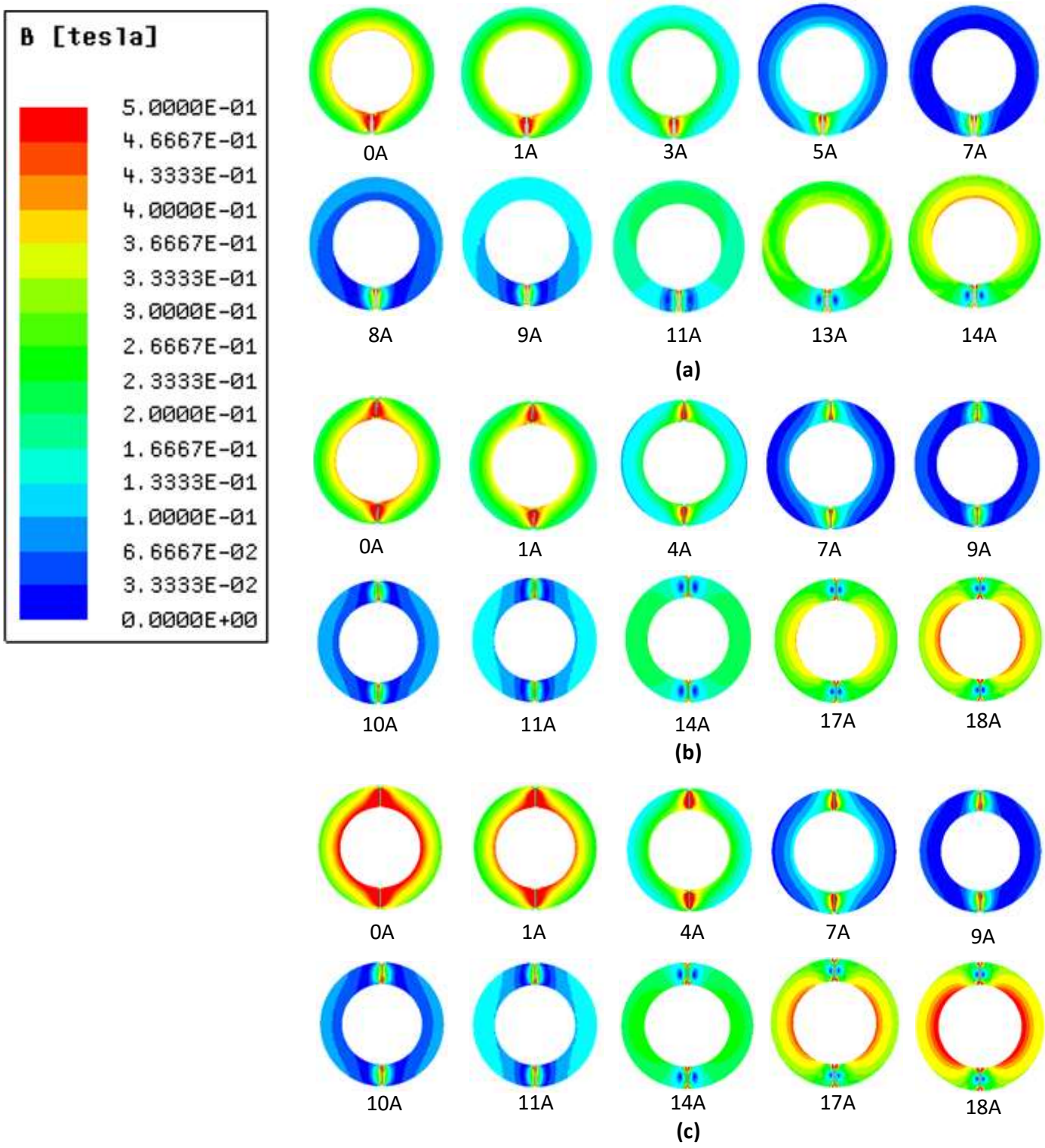


Fig. 2. The magnitude of flux density (i.e. B) when the DC current increases for the core of the: (a) PM-TPI, (b) DPM-TPI-1, and (c) DPM-TPI-2.

Another important design aspect of PM power inductor is to prevent the demagnetization of PM. The demagnetization occurs when there is a reverse field (H) larger than a certain value, which is specific for the type of PM used. For NdFeB-N35EH PM utilized in this paper, the demagnetization occurs when the reverse H-field applied to the PM is larger than 1989 kA/m at 26.8 °C. Fig. 4 shows the H-filed distribution of PMs of DPM-TPI-2 when the DC current is 21 A. It can be observed from Fig. 4 that the maximum H value is 734.4 kA/m, which is far from the demagnetization value 1989 kA/m. This indicates that the PMs will not be demagnetized under the operation conditions in this paper.

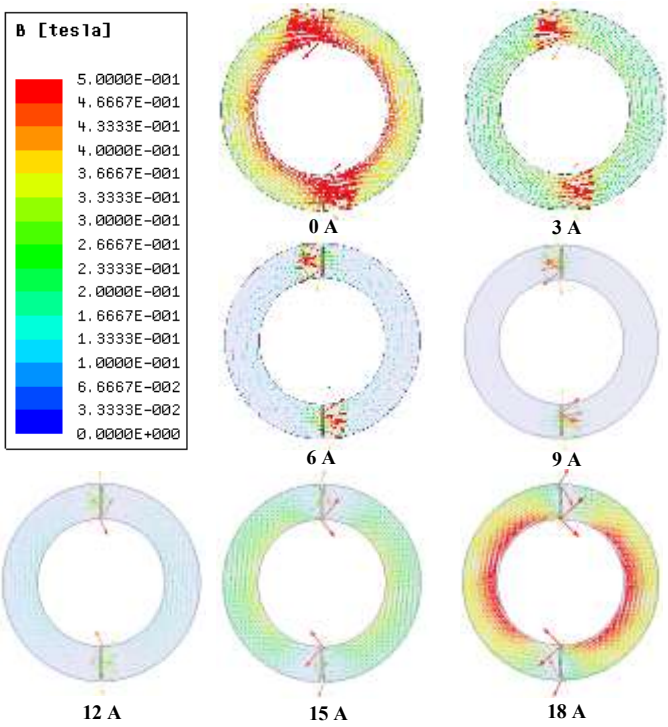


Fig. 3. The vector of flux density (i.e. B) in the core of DPM-TPI-2 when the DC current increases from 0A to 18A.

## IV. Conclusion

Different PM distribution patterns for toroid power inductor are modelled and evaluated to compare their effects on the performance metrics of the power inductor, namely, saturation current and inductance. The proposed structure with multi-PMs and gaps inserted evenly through the core of the power inductor allows to achieve more effective and more uniform flux cancellation with possible small drop in inductance value. This effective cancellation helps to increase the saturation current of the power inductor. By reducing or tuning the gaps sizes with PMs, the inductance value can be close to that of the structure with single gap and a single PM. The proposed inductor design method in this work allows to achieve high saturation current and high inductance density simultaneously, which is highly desired and important for high power density application.

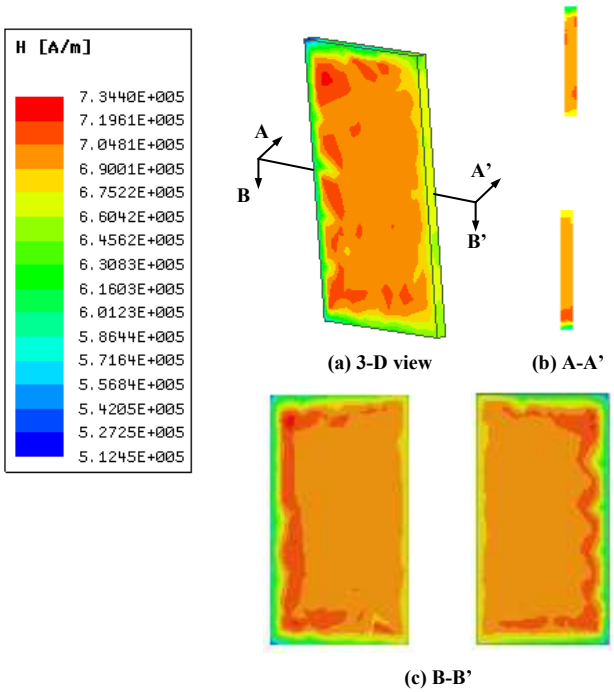


Fig. 4. The demagnetization field of the PMs of DPM-TPI-2 when the DC current is 21A: (a) 3-D view, (b) and (c) cross-sectional views.


## Acknowledgment

This material is based upon work supported in part by the National Science Foundation under Grant No. 1708690. Any opinions, findings and conclusions or recommendations expressed in this material are those of the author(s) and do not necessarily reflect the views of the National Science Foundation.


## References


[1] J. Wyk and F. Lee, "On a Future for Power Electronics," *IEEE Journal of Emerging and Selected Topics in Power Electronics*, vol. 1, no. 2, pp. 59-72, June 2013.

[2] S. Chen, T. Liang, L. Yang, and J. Chen, "A boost converter with capacitor multiplier and coupled inductor for ac module applications," *IEEE Transactions on Industrial Electronics*, vol. 60, no. 4, pp. 1503–1511, April 2013.

[3] Z. Dang and J. A. Abu Qahouq, "Evaluation of high-current toroid power inductor with NdFeB magnet for DC–DC power converters," *IEEE Transactions on Industrial Electronics*, vol. 62, no. 11, pp. 6868-6876, November 2015.

[4] J. A. Abu Qahouq and Z. Xia, "Single-perturbation-cycle online battery impedance spectrum measurement method with closed-loop control of power converter," *IEEE Transactions on Industrial Electronics*, vol. 64, no. 9, pp. 7019-7029, September 2017.

[5] M. Wang, J. Li, K. Ngo, and H. Xie, "A Surface-mountable microfabricated power inductor in silicon for ultracompact power supplies," *IEEE Transactions on Power Electronics*, vol. 26, No. 5, pp. 1310-1315, May 2011.

[6] W. Huang and J. A. Abu Qahouq. "An online battery impedance measurement method using DC–DC power converter control," *IEEE Transactions on Industrial Electronics*, vol. 61, no. 11, pp. 5987-5995, June 2014.

[7] J. A. Abu Qahouq and Y. Cao . “Control scheme and power electronics architecture for a wirelessly distributed and enabled battery energy storage system,” *Energies*, vol. 11, no. 7, pp. 1-20, July 2018. https://doi.org/10.3390/en11071887.

[8] V. Sung and W. Odendaal, “Litz wire pulsed power air core coupled inductor,” *IEEE Transactions on Industry Applications*, vol. 51, no. 4, pp. 3385-3393, July-August 2015.

[9] J. Ewanchuk and J. Salmon, “Three-limb coupled inductor operation for paralleled multi-level three-phase voltage sourced inverters,” *IEEE Transactions on Industrial Electronics*, vol. 60, no. 5, pp. 1979–1988, May 2013.

[10] Y. Cao and J. A. Abu Qahouq. “Analysis and evaluation of a dual-variable closed-loop control of power converter with wireless and non-wireless power transfer,” *IEEE Transactions on Industrial Electronics*, pp. 1-1, June 2018, early access, (DOI: 10.1109/TIE.2018.2842777).

[11] M. Saidani, and M. Gijs, “Cubic millimeter power inductor fabricated in batch-type wafer technology,” *Journal of Microelectromechanical Systems*, vol. 12, no. 2, pp. 172-178, April 2003.

[12] Y. Cao and J. A. Abu Qahouq. “Evaluation of bi-directional single-inductor multi-input battery system with state-of-charge balancing control,” *IET Power Electronics*, August 2018, early access, (DOI: 10.1049/iet-pel.2018.5474).

[13] I. Josifovic, J. Gerber, and J. Ferreira, “New double-sided SMT power inductor,” *IEEE Transactions on Industry Applications*, vol. 49, no. 4, pp. 1637-1648, July-August 2013.

[14] Z. Xia, J. A. Abu Qahouq, E. Phillips, and R. Gentry, “A simple and upgradable autonomous battery aging evaluation and test system with capacity fading and AC impedance spectroscopy measurement,” in *APEC*, pp. 951-958, March 2017.

[15] Y. Li, Y. Xie, R. Chen, L. Han, D. Chen, and H. Su, “A multilayer power inductor fabricated by cofirable ceramic/ferrite materials with LTCC technology,” *IEEE Transactions on Components, Packaging and Manufacturing Technology*, vol. 7, no. 9, pp. 1402-1409, September 2017.

[16] T. Sato, K.Watanabe, H. Igarashi, T. Matsuo, T. Mifune, K. Kawano, M. Suzuki, Y. Uehara and A. Furuya, “3-D Optimization of Ferrite Inductor Considering Hysteresis Loss,” *IEEE Transactions on Magnetics*, vol. 49, no. 5, pp. 2129-2132, May 2013.

[17] Z. Xia and J. A. Abu Qahouq, “Method for online battery AC impedance spectrum measurement using dc-dc power converter duty-cycle control,” in *APEC*, pp. 951-958, March 2017.

[18] G. Capua and N. Femia, “A novel method to predict the real operation of ferrite inductors with moderate saturation in switching power supply applications,” *IEEE Transactions on Power Electronics*, vol. 31, no. 3, pp. 2456–2464, March 2016.

[19] Z. Xia and J. A. Abu Qahouq, “An online battery impedance spectrum measurement method with high frequency resolution,” in *APEC*, pp. 1930-1933, March 2018.

[20] R. Salas and J. Pleite, “Equivalent Electrical Model of a Ferrite Core Inductor Excited by a Square Waveform Including Saturation and Power Losses for Circuit Simulation,” *IEEE Transactions on Magnetics*, vol. 49, no. 7, pp. 4257-4260, July 2013.

[21] Z. Xia and J. A. Abu Qahouq, “State-of-health indication method for li-ion batteries,” in *APEC*, pp. 1829-1833, March 2018.

[22] S. Yoon, T. Dang, N. Lai, and J. Park, “Efficient Wi-Fi power amplifier LTCC module using a buck converter with a power inductor implemented in ferrite-filled PCB technology,” *IEEE Transactions on Components, Packaging and Manufacturing Technology*, vol. 5, no. 7, pp. 887-894, July 2015.

[23] Z. Dang and J. A. Abu Qahouq, “Permanent-magnet coupled power inductor for multiphase dc-dc power converters,” *IEEE Transactions on Industrial Electronics*, vol. 64, no. 3, pp. 1971-1981, November 2017.

[24] X. Fang, R. Wu, L. Peng, and J. Sin, “A novel integrated power inductor with vertical laminated core for improved L/R ratios,” *IEEE Electron Device Letters*, vol. 35, no. 12, pp. 1287-1289, December 2014.

[25] “3C96 material specification,” [Online]. Available: https://www.ferroxcube.com/en-global/ak_material/index/power_conversion, accessed on July 1, 2018.

[26] “Sintered NdFeB Magnets,” [Online]. Available: http://www.tridelta.de/viomatrix/imgs/download/sintered__ndfeb_magnets.pdf, accessed on July 1, 2018.